PAPER

Development of an improved wearable device for core body temperature monitoring based on the dual heat flux principle

IOP Publishing | Institute of Physics and Engineering in Medicine Physiological Measurement

Physiol. Meas. **38** (2017) 652–668 https://doi.org/10.1088/1361-6579/aa5f43

Development of an improved wearable device for core body temperature monitoring based on the dual heat flux principle

Jingjie Feng[1], Congcong Zhou[1], Cheng He[1], Yuan Li[1] and Xuesong Ye[1,2]

[1] Biosensor National Special Laboratory, College of Biomedical Engineering and Instrument Science, Zhejiang University, Hangzhou 310027, People's Republic of China

[2] State Key Laboratory of CAD and CG, Zhejiang University, Hangzhou 310027, People's Republic of China

E-mail: yexuesong@zju.edu.cn

Received 8 July 2016, revised 20 January 2017
Accepted for publication 8 February 2017
Published 17 March 2017

Abstract

Objective: In this paper, a miniaturized wearable core body temperature (CBT) monitoring system based on the dual heat flux (DHF) principle was developed. *Approach:* By interspersing calcium carbonate powder in PolyDimethylsiloxane (PDMS), a reformative heat transfer medium was produced to reduce the thermal equilibrium time. Besides, a least mean square (LMS) algorithm based active noise cancellation (ANC) method was adopted to diminish the impact of ambient temperature fluctuations. Theoretical analyses, finite element simulation, experiments on a hot plate and human volunteers were performed. *Main results:* The results showed that the proposed system had the advantages of small size, reduced initial time (~23.5 min), and good immunity to fluctuations of the air temperature. For the range of 37–41 °C on the hot plate, the error compared with a Fluke high accuracy thermometer was 0.08 ± 0.20 °C. In the human experiments, the measured temperature in the rest trial (34 subjects) had a difference of 0.13 ± 0.22 °C compared with sublingual temperature, while a significant increase of 1.36 ± 0.44 °C from rest to jogging was found in the exercise trial (30 subjects). *Significance:* This system has the potential for reliable continuous CBT measurement in rest and can reflect CBT variations during exercise.

Keywords: core body temperature, heat flux, active noise cancellation, wearable

(Some figures may appear in colour only in the online journal)

1. Introduction

Core body temperature (CBT), regarded as the operating temperature in deep structures of the body, is one of the vital physiological parameters indicating people's function and health condition. CBT usually keeps steady at the range of 36.5–37.5 °C, whereas skin temperature is susceptible to the fluctuation of external environment. It has been found that the circadian rhythm of CBT is relevant to human locomotive activities (Satlin *et al* 1995, Byrne and Lim 2007), cognitive performance and physiological phenomena (Freedman 2014, Nybo *et al* 2014). Moreover, CBT offers reliable diagnoses on some disorders or symptoms such as heat stroke (Epstein and Roberts 2011) and fever (Conti *et al* 2004). Hence the long-term continuous measurement of CBT is of great significance.

Direct measurements of CBT require the insertion of a probe (e.g. pulmonary artery catheter, oesophagus, and rectum), which is inconvenient for long-term continuous monitoring. Ingestible temperature sensors represent a valid index of CBT, while the main restrictions are the delay time after ingestion, interference by fluid and food, influence of gastrointestinal motility, electromagnetic interference and disposability (Kolka *et al* 1993, Byrne and Lim 2007, Teunissen *et al* 2012). Noninvasive methods are more appealing due to the convenience. However, simply taking the skin temperature as a surrogate for CBT is not reliable, since it is more prone to the forced convection (Richmond *et al* 2013), skin thickness, and sensor site (Mendt *et al* 2016). Other noninvasive techniques based on the heat flux theory have been introduced in the last decades. The zero heat flux (ZHF) method (Fox *et al* 1973, Nemoto and Togawa 1988, Yamakage and Namiki 2003, Steck *et al* 2011, Teunissen *et al* 2011, Eshraghi *et al* 2014) uses an insulation layer to prevent the heat loss from the tissue, and the measured temperature is thought to be equivalent to the CBT when the isothermal tunnel is built. Since extra heaters are required, the ZHF method usually consumes substantial amount of energy, which is a major hurdle for those battery-powered wearable devices imposing lifetime constraints. Compared with the ZHF method, the single heat flux (Gunga *et al* 2008, 2009) and dual heat flux (DHF) (Yuan 2009, Kitamura *et al* 2010, Sim *et al* 2012, Saurabh *et al* 2014, Huang *et al* 2016) (SHF/DHF) methods are more power-efficient. However, the measurement time is usually longer than that of the ZHF method, and the systems based on the heat flux methods mentioned above are large in size with cumbersome transmission cables. Thus, for users who cared about CBT fluctuations in daily routines (e.g. fitness and jogging enthusiasts during exercise), improved approaches such as the acceleration of the thermal equilibrium and the miniaturization of the system should be prompted, to make the device wearable and convenient, especially under field conditions.

In this paper, a miniaturized core body temperature monitoring system (CBTMS) was implemented. A reformative material composed of calcium carbonate and PDMS was adopted to improve the thermal response, as well as provide a soft and natural attachment to the skin. A least mean square (LMS) algorithm based active noise cancellation (ANC) method was applied to diminish the artifact of the unstable thermal state caused by the strong convective air.

2. Materials and methods

2.1. An overview of the CBTMS

The prototype of the temperature probe based on the DHF method was shown in figure 1(a). The probe consisted of two blocks whose diameters were both 34 mm. The heights of the two blocks were 10 mm (Block 1) and 4 mm (Block 2). The battery-powered wearable CBTMS was fixed by an elastic hairband (figure 1(b)). The temperature probe was attached to the forehead. The gap between the two blocks was 5 mm. Each block was covered by a medical sponge cap.

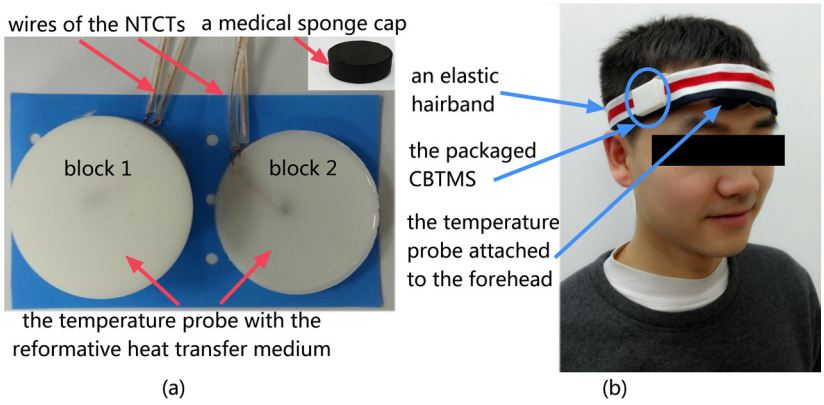

Figure 1. (a) The temperature probe with the reformative heat transfer medium and the cap made of the medical sponge. (b) The CBTMS prototype worn by a participant under test.

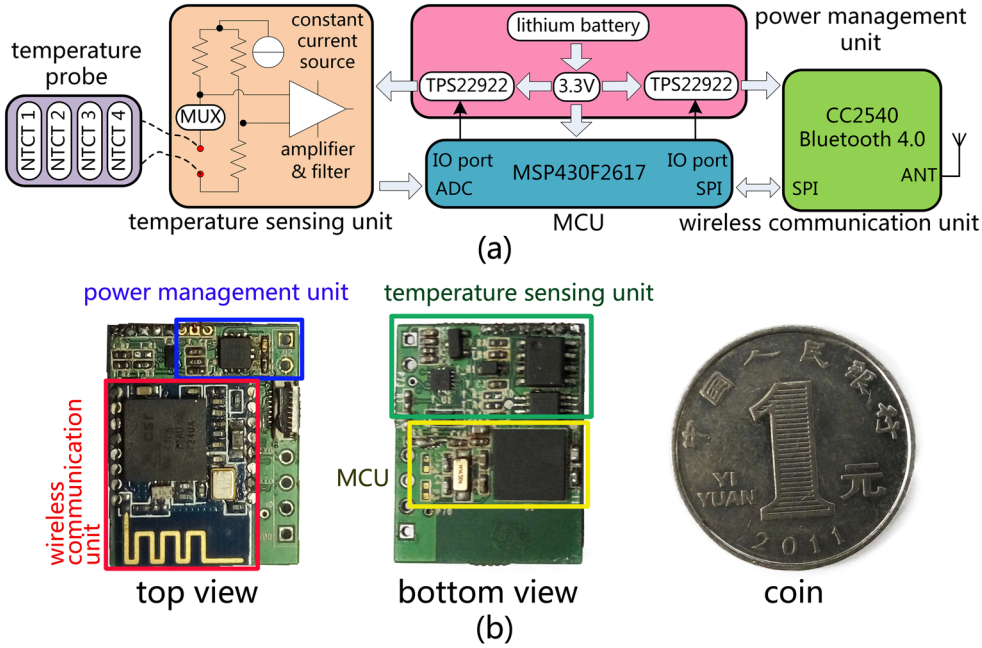

Figure 2. (a) The block diagram of the wearable CBTMS. (b) The top and bottom views of the print circuit board of the CBTMS.

The proposed CBTMS consisted of five units, namely the temperature probe, temperature sensing unit, microcontroller unit (MCU), power management unit and wireless communication unit. The block diagram of the CBTMS was depicted in figure 2(a). The probe included four thin negative temperature coefficient (NTC) thermistors (MF51E from CANTHERM). The NTC thermistor 1 (NTCT1) and NTCT3 were placed on the bottom of Block 1 and Block 2 respectively. NTCT2 and NTCT4 were placed on the top of Block 1 and Block 2 respectively. The four NTCTs were connected in parallel and controlled by a quad analog switch (TS3A4751 from TI), which provided a negligible on-state resistance. Each NTCT

was chosen alternatively to access the temperature sensing unit. The selected NTCT and other three low-temperature-coefficient precision resistors constituted a Wheatstone bridge circuit. With a zero temperature coefficient constant current source composed of LM334M (TI) and IN4148 (Semtech Electronics), the impedance change of the NTCT was converted to the voltage variation. Afterwards, it was amplified and low pass filtered to eliminate the high frequency noise. A high gain accuracy operational amplifier (INA321, Burr-Brown from TI) with 10 times gain was employed. The signals sampled at 0.5 Hz were digitized by a 12 bit ADC block, and processed in the MCU (MSP430F2617 from TI), then fed to the wireless communication unit (Bluetooth 4.0 module, CC2540 from TI) for transmission. Bluetooth low energy (BLE) technology was adopted here for low power consumption. What's more, two ultra-low power switches (TPS22922 from TI) controlled by the MCU were adopted in the power management unit. The power supplies of the temperature sensing unit and wireless communication unit could be selectively turned off when they were not occupied. And the power consumption of the CBTMS was further decreased.

The designed print circuit board (figure 2(b)) was in size of 19 mm $\times$ 24 mm, and the system was powered by a rechargeable lithium battery (3.7 V, 60 mAh). The utilization of the low power strategies (controllable power switches and BLE technology) met the demand of energy efficiency for power-constrained wearable systems. And the CBTMS was more compact without transmission cables hindering daily activities.

2.2. The heat transfer medium

PDMS (SYLGARD 184 silicone elastomer from Dow Corning) was used as the heat transfer medium of the probe, since it was flexible, biocompatible and highly hydrophobic. The probe could be exposed to sweat and attached to skin softly. Viscoelasticity was another major reason for which PDMS was chosen. PDMS acted like a viscous liquid when the Base and the Curing agent were mixed together, and an elastic solid after solidification. This special mechanical property made it easy to form almost any shapes, and various structures could be implemented flexibly.

Furthermore, the way to increase the thermal conductivity was studied, in order to overcome the drawback of the long heat balance time of the DHF method. Calcium carbonate powder with a reported thermal conductivity of 2.467 W $m^{-1} \cdot K$ was chosen to mix with the PDMS in a specified volume ratio, and the probe (figure 1(a)) was degassed before solidification to minimize the air gap.

2.3. LMS adaptive filter based ANC method

Ambient temperature (T_{air}) fluctuations could disturb the thermal equilibrium, and affect the CBT assessment. The ANC method helped mitigate the artifacts and diminish the impact caused by the changed ambient temperature. It sought much attention since the characteristics of adjustable filter coefficients and changeable bandwidth made the signal processing more flexible (Hansen 2002).

In this approach, the LMS adaptive filter was chosen for its stability, relatively small amount of computation (Haykin and Widrow 2003, Han and Kim 2012) and good compatibility with resource-limited wearable systems. The principle was presented in the appendix.

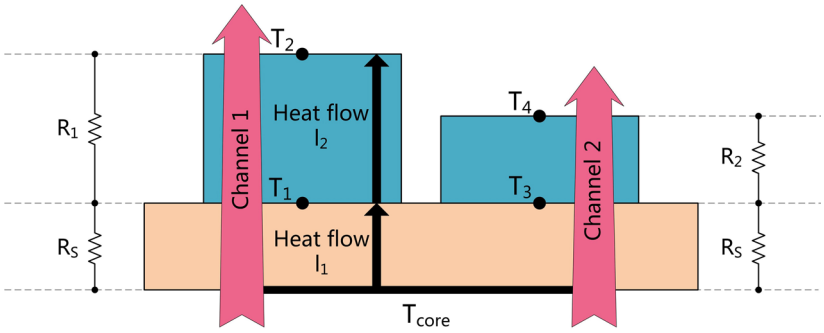

Figure 3. The model of CBT measurement based on the DHF method.

2.4. The principle of CBT measurement

The estimation of CBT was based on the model illustrated in figure 3. The orange part represented the skin and subcutaneous tissue layer of the human body, while the blue parts attached upside stood for the temperature probe. There was always a temperature gradient between the deep tissue inside the body and the surface of the skin and subcutaneous tissue layer in vertical direction, since the CBT was typically higher than the skin temperature.

Taking the heat fluxes in two channels into consideration, for a steady-state model, the CBT could be finally calculated by equation (1). The detailed derivation was presented in the appendix.

$$T_{\text{core}} = T_1 + \frac{(T_1 - T_2)(T_1 - T_3)}{K(T_3 - T_4) - (T_1 - T_2)}, K = \frac{R_1}{R_2} \tag{1}$$

Where K was defined as the ratio of thermal resistances R_1 and R_2. Theoretically, K should also be equal to the ratio of the thickness of those two channels, if the probe was made of the same material with homogeneous properties. However, in fact we found that K did not solely depend on the ratio of two channels' thickness due to the existence of the horizontal heat flow. Therefore, K should be derived practically rather than theoretically. On the other hand, the horizontal heat flow was mitigated by two means in this study, in order to better coincide with the fundamental model: (1). the temperature probe was covered with the medical sponge to provide certain heat isolation, and (2). the division of two separate blocks of the probe prevented the direct transverse heat exchange between T_1 and T_3.

2.5. FEM simulation

The finite element method (FEM) used subdivision of a whole problem domain into simpler parts called finite elements to mathematically model and numerically solve complex problems in practical applications. With the help of an analysis software COMSOL Multiphysics™, the heat transfer simulation was conducted to assess the feasibility of the DHF method.

Huang and Chen (2010) simulated the probe whose sensors were integrated in a single block. Here, four sensors were embedded in two separate blocks to weaken the impact of the horizontal heat conduction. The temperature on the bottom of the skin and subcutaneous

tissue layer was set to T_{core} as the initial condition. The periphery of the skin and subcutaneous tissue layer was set to be thermal insulated. Regarding the boundary conditions, both convective heat flux and surface-to-ambient radiation on the top of the skin and subcutaneous tissue layer were considered, because the skin was usually exposed to the ambient environment.

$$-\lambda\left(\frac{\partial T}{\partial x}+\frac{\partial T}{\partial y}+\frac{\partial T}{\partial z}\right)=h(T_{air}-T) \tag{2}$$

$$e_b(T)=\varepsilon\sigma(T_{air}^4-T^4) \tag{3}$$

These two boundary conditions could be expressed as the Newton's law of cooling and the Stefan–Boltzmann's law, namely equations (2) and (3) (Lienhard and Lienhard 2006). The top and periphery of the probe shared the same thermal radiation as the boundary conditions.

For a given T_{core}, K could be derived from equation (1) as follows.

$$K=\frac{(T_{core}-T_3)(T_1-T_2)}{(T_{core}-T_1)(T_3-T_4)} \tag{4}$$

In this model, the accuracy of temperature data was set to the fourth decimal place, and the mesh setting was in physics-controlled sequence type with normal element size. The geometric dimension of the probe kept the same as the prototype described in section 2.1. The thickness of the skin and subcutaneous tissue layer (H_{st}) varied from 4 mm to 20 mm, while the length and width were 75 mm and 45 mm respectively.

A stationary state simulation was performed to observe its temperature distribution at T_{core} of 37.0 °C and T_{air} of 25.0 °C. Furthermore, the relationships between K and other variables (i.e. T_{core}, T_{air}, H_{st}) were simulated by MATLAB via the interface offered by COMSOL.

2.6. Tests of the temperature probe

The calibrated NTCTs were tested in a thermostatic water tank, and compared with a Fluke high accuracy digital thermometer 1502A, which has a high temperature resolution of 0.001 °C and a low temperature coefficient of resistance about 1 ppm $°C^{-1}$. The probe was then well packaged. The initial time, measured from the time when the probe was attached to the forehead, to the time when the temperature of the sensor placed on the bottom was stable ($< \pm 0.1$ °C variation), was used to compare the thermal response of the probes made of different heat transfer mediums (PDMS, calcium carbonate mixed PDMS).

2.7. Experiments on a hot plate

A hot plate (Super-Nuova series from Thermo Scientific) was adopted as the heat source of CBT. Besides, another PDMS (Base: Curing agent = 10: 1) layer (noted as PDMS_skin) whose thickness was 5 mm, was used to imitate the skin and subcutaneous tissue layer, as they shared the close thermal conductivities of 0.15 W $m^{-1} \cdot K$ and 0.17 W $m^{-1} \cdot K$. The probe which attached closely to PDMS_skin was utilized to assess the temperature of the hot plate. The temperatures of the NTCTs (T_{1_meas}–T_{4_meas}) were sampled at 0.5 Hz. K was calculated by equation (4) when the values were steady. The derived K was then exerted to deduce the estimated CBT (T_{core_est}).

An experiment imitated the circumstance of fever was carried out to test the accuracy of the CBTMS from 37 °C to 41 °C. At first, the temperature of the hot plate was set to 36 °C,

and its exact value (T_{core_meas}) was measured by a high precision Pt thermometer. The room temperature (T_{air}) was around 26 °C. The temperature of the hot plate was increased by 1 °C about 50 min after each thermal equilibrium.

Another experiment imitated the sudden appearance of unstable thermal status was performed to verify the effect of the ANC method. μ mentioned in the appendix was valued as 0.08, $w(n)$ was updated by the gradient descent algorithm. $d(n)$ was preprocessed by a digital smooth filter to remove the high frequency noise. Another thermometer was used to record T_{air} at 0.5 Hz. Acute fluctuations of the ambient temperature (~1.1 °C min^{-1}) was manually established by manipulating the air conditioner.

The differences between T_{core_est} and T_{core_meas} were calculated to evaluate the accuracy of the CBTMS.

2.8. Trials on human volunteers

After the validation on the hot plate, the CBTMS was tested on humans in two trials (the rest trial and the exercise trial). Sublingual temperature (T_{sub}) was an applicable access for near-core temperature measurement (Höcker *et al* 2012) and was a close reflection of CBT in the absence of a pulmonary artery catheter (Hooper and Andrews 2006). Thus, T_{sub} was measured by a digital thermometer (SureTemp® Plus 690 from Welch Allyn) as reference. Informed consent was obtained from all the participants, noting that no ingestion of food or fluid was allowed during both trials. The experiments were approved by the Ethical Committee of Zhejiang University.

34 healthy subjects (30 males, 4 females, 26.8 ± 2.1 years old) participated in the rest trial indoors. The room temperature was around 26 °C, and the relative humidity was 50–60%. First, subjects were required to wear the CBTMS for about 50 min in sitting position and resting state, in order to get used to the attachment of the probe and wait for the establishment of the thermal equilibrium. Afterwards, T_{core_est} was sampled at 0.5 Hz while T_{sub} was measured every 10 min for three times. During every T_{sub} measurement, the probe tip was quickly placed under the subject's tongue in the left posterior sublingual pocket with lips closed. The value was recorded after stabilization (~8 s). T_{core_est} was filtered and averaged, then compared with the average T_{sub} to confirm the consistency. A Bland–Altman diagram (Bland and Altman 1995) was constructed to quantify the deviation between the processed T_{core_est} and T_{sub}. The average value of two compared temperatures was depicted against their difference.

30 male subjects (27.0 ± 2.1 years) completed the exercise trial on a playground. The outdoor temperature was 25–30 °C, and the relative humidity was about 70%. The whole trial started with a habituation stage of about 50 min (subjects sat on a chair), then continued with a measurement stage of 60 min, which included three sessions (10 min rest, 30 min jogging and 20 min passive recovery). The rest and recovery sessions were performed in sitting position, while the jogging session started at a pace of 5–7 km h^{-1} for the first 15 min, then increased to 7–9 km h^{-1} for the next 10 min, and ended with 9–11 km h^{-1} for the last 5 min. The speed was controlled by the participant using a smart phone with GPS module integrated. During the measurement stage, T_{core_est} was sampled at 0.5 Hz by the CBTMS. In this trial, CBT was expected to change significantly, thus the sensitivity of the CBTMS could be evaluated. The repeated measures ANOVA was conducted on the averaged T_{core_est} of the last 1 min of each session, to determine significant changes during a session transition. Besides, both the first and the last 1 min averaged T_{core_est} of each session were tested by paired t-tests, to determine differences between the start and the end within a session. Significance level was set at $p < 0.05$.

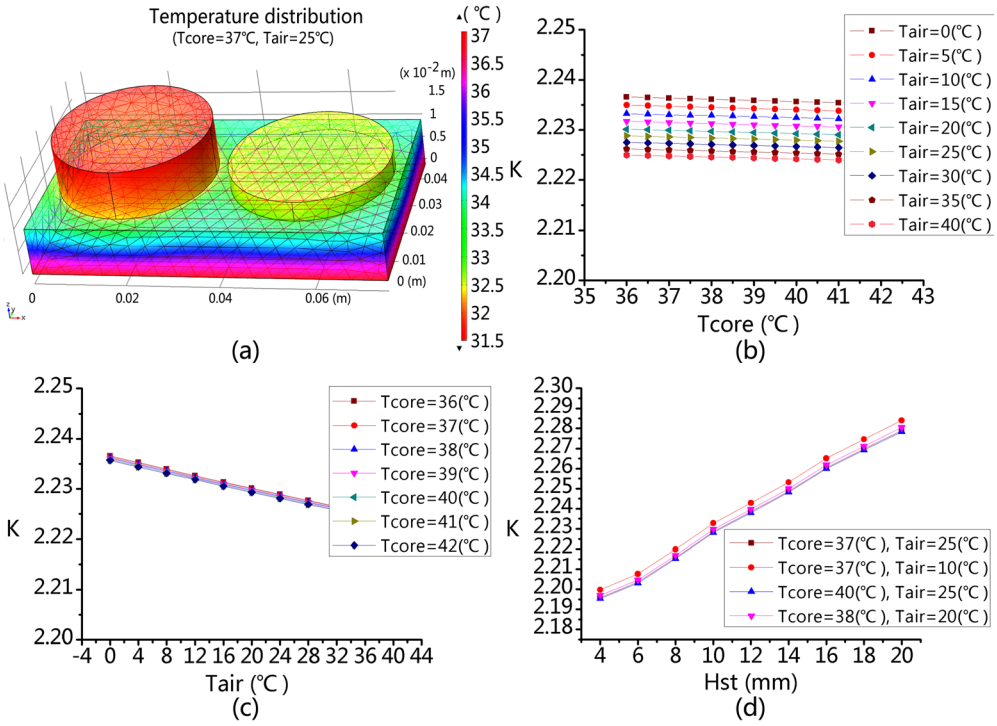

Figure 4. (a) The temperature distribution of the model in the stationary state study. (b) The relationship between K and T_{core} in different ambient temperatures. (c) The relationship between K and T_{air} in different CBTs. (d) The relationship between K and the thickness of the skin and subcutaneous tissue layer in different CBTs and ambient temperatures.

3. Results

3.1. FEM simulation

The temperature distribution of the model in the steady state (T_{core} 37.0 °C, T_{air} 25.0 °C) was displayed in figure 4(a). It showed that the temperature reduced obviously along the vertical direction (z axis), while a slight temperature gradient descent was found in horizontal (x–y plan) due to the introduction of the heat convection and surface-to-ambient radiation.

Figure 4(b) illustrated that K stayed consistent despite of the change of T_{core} from 36.0 °C to 42.0 °C when T_{air} was constant. Besides, K kept almost steady (<0.01 change) even if T_{air} fluctuated from 0.0 °C to 40.0 °C in a wide range. Figure 4(c) depicted that K also showed its stability (~0.01 change) regardless of T_{air} variation in a wide T_{core} range. The relationship between K and H_{st} was demonstrated in figure 4(d). Four groups with different T_{core} and T_{air} were studied. There was a same trend among four curves, and K was proportional to H_{st} from 4 mm to 20 mm. However, the change of K was almost 10 times larger compared with that in figures 4(b) and (c). It meant K was more easily affected by the thickness of the skin and subcutaneous tissue layer rather than the CBT and ambient temperature.

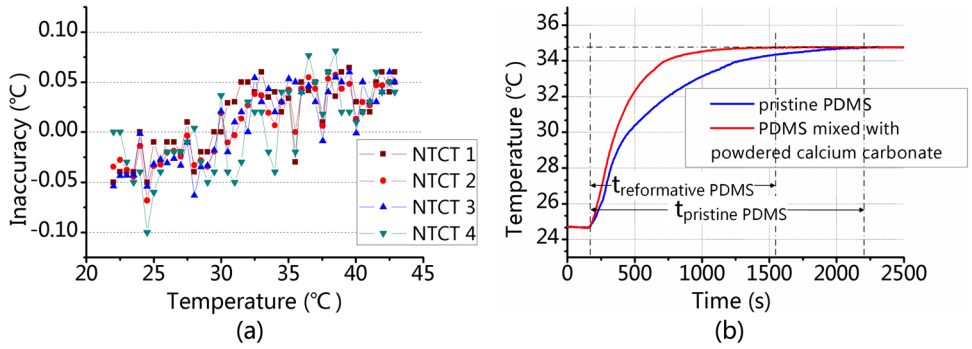

Figure 5. (a) The measurement inaccuracy of the NTCTs compared with Fluke 1502A. (b) The thermal response of the probes made of different heat transfer mediums (PDMS, calcium carbonate mixed PDMS).

3.2. Tests of the temperature probe

Figure 5(a) showed the measurement inaccuracy of the NTCTs compared with the 1502A. In the designed working range of 22.0–42.0 °C, the errors were 0.015 ± 0.036 °C, 0.009 ± 0.034 °C, 0.008 ± 0.037 °C, 0.002 ± 0.042 °C, respectively. Four NTCTs shared the temperature resolution of 0.002 °C, while the average inaccuracy was 0.009 ± 0.037 °C. The high precision of the NTCTs ensured the reliability of the CBTMS.

Figure 5(b) indicated the thermal response of the probes. It appeared that the initial time of the probe with the calcium carbonate mixed was about 32.1% (23.5 min: 34.6 min) faster than that of the probe made of pristine PDMS.

3.3. Experiments on a hot plate

The curves of T_{core_meas}, T_{1_meas}–T_{4_meas}, and T_{core_est} during the experiment were depicted in figure 6(a). They revealed that in the range of 37–41 °C, the inaccuracy of the estimated CBT was low (−0.08 ± 0.12 °C at 37 °C, −0.10 ± 0.15 °C at 38 °C, 0.06 ± 0.17 °C at 39 °C, 0.08 ± 0.12 °C at 40 °C, and 0.13 ± 0.17 °C at 41 °C, respectively). The average error was 0.08 ± 0.20 °C in 37–41 °C. Besides, the probe showed good traceability and relatively quick response when the temperature of the hot plate started to change sharply.

Figure 6(b) displayed the original temperature curves. The change of T_{1_meas}–T_{4_meas} was consistent with that of T_{air}. Ambient temperature fluctuations occurred from 2450 s to 4125 s. Since the thermal status was disequilibrated, the T_{core_est} curve distorted obviously and deviated from T_{core_meas} a lot (error 0.40 ± 0.76 °C, 3.2 °C max deviation). Figure 6(c) illustrated that after utilizing the adaptive filter, sharp changes of T_{1_meas}–T_{4_meas} were suppressed, while T_{core_est} coordinated much better with T_{core_meas}. With the ANC method applied, the CBTMS became more robust to predict CBT even if the thermal equilibrium was disturbed (error reduced to 0.31 ± 0.44 °C). Once the heat balance was established again (after ~4850 s, recovery time ~10 min), the measurement inaccuracy became −0.08 ± 0.10 °C.

3.4. Trials on human volunteers

The average T_{core_est} of all the subjects in the rest trial was 36.77 ± 0.31 °C.A Bland–Altman plot for T_{core_est} and T_{sub} was displayed in figure 7(a), which depicted a difference of 0.13 ± 0.22 °C. The temperature measured by the CBTMS had adequate consistency with the sublingual temperature in resting state.

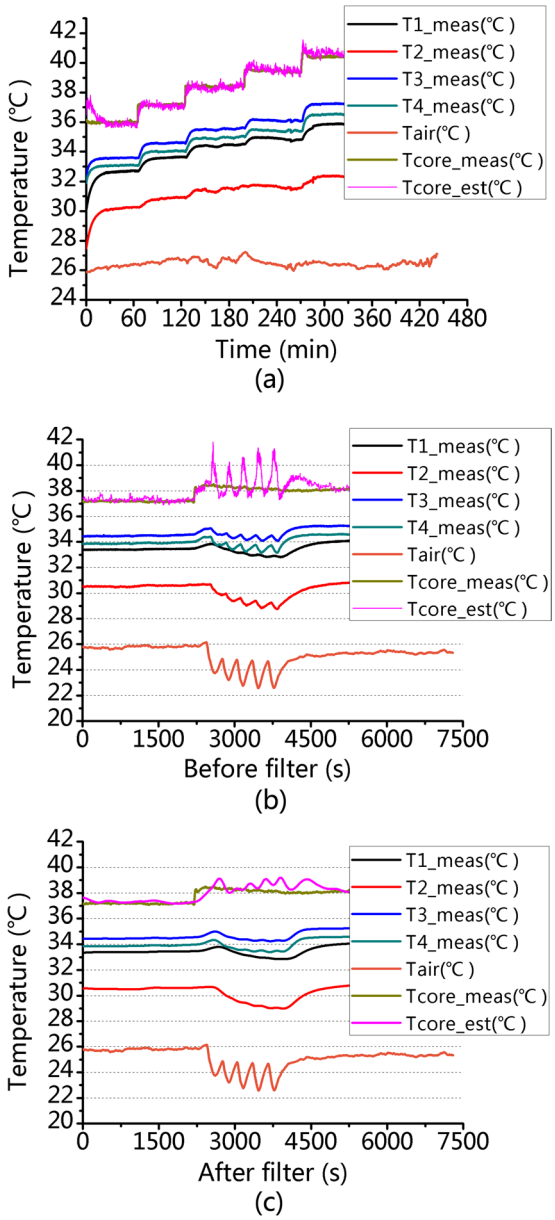

Figure 6. (a) Experiment of the measurement accuracy on the hot plate. The temperature rose in the step of 1 °C. (b) The curves of T_{core_meas}, T_{1_meas}–T_{4_meas}, T_{core_est} and T_{air} before utilizing the LMS adaptive filter. (c) The original curves of T_{core_meas}, T_{air} and the curves of T_{1_meas}–T_{4_meas}, T_{core_est} after utilizing the LMS adaptive filter. Noting that the temperature variations between 2450 s and 4125 s were manually established.

An overview of the measured temperatures of Subject No.17 was elucidated in figure 7(b). T_{core_est} rose clearly from 36.84 ± 0.04 °C in rest, to 38.04 ± 0.11 °C during the last 1 min jogging, and decreased to 36.97 ± 0.10 °C after 20 min recovery. For all the subjects, the average difference of T_{core_est} between the last 1 min of the rest and jogging sessions was

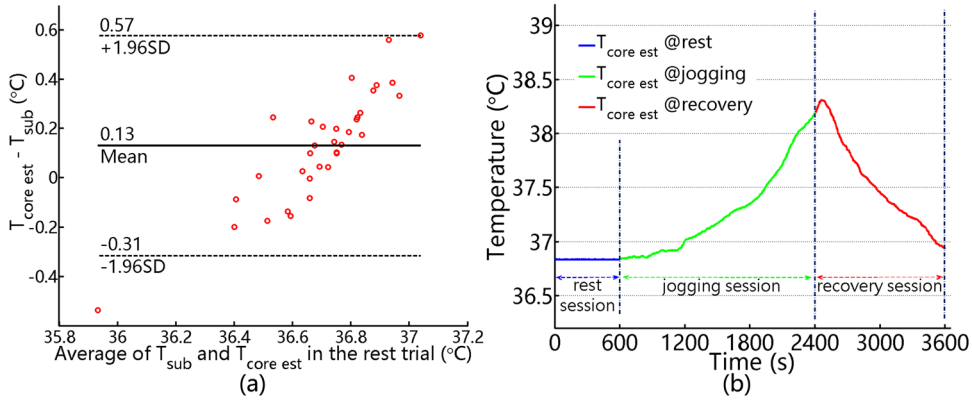

Figure 7. (a) The Bland–Altman plot for T_{core_est} and T_{sub} in the rest trial. (b) The T_{core_est} pattern of Subject No. 17 during the exercise trial.

1.36 ± 0.44 °C. ANOVA showed that T_{core_est} in the last 1 min of the three sessions were significantly different. It rose significantly ($n = 30$, $p < 0.05$) after jogging and decrease significantly ($n = 30$, $p < 0.05$) when the recovery session terminated. Thus, the manipulation of changing CBT in this trial succeeded. It implied that the CBTMS placed on the forehead could reflect the variation of CBT.

4. Discussion

CBT is a reliable barometer for human health status. It would be helpful if a wearable thermometry is used in daily health management. Yamakage and Namiki (2003) mentioned two deep body thermometers (CTM-205 and CM-210) which were applied in clinical fields but not wearable. Eshraghi *et al* (2014) reported a temperature monitoring system (3M SpotOn) which needed external AC power supply, and the dimensions of its control unit were 93 mm high and 71 mm wide. Huang *et al* (2016) developed a cable-transmission thermometry prototype with only the basic storage function implemented, and data loss was found due to the cable disconnecting after abrupt movements. Compared with these systems, our CBTMS was smaller, more compact packaged, convenient and free of redundant transmission wires, which was adequate to work as a sensor node of wireless body area network (WBAN) for health monitoring.

FEM simulation could examine the DHF method's capability and offer guidelines for further designs. In practice, CBT could be obtained within acceptable errors if K kept stable. The simulation showed that K was more easily affected by H_{st} rather than T_{air}. An upward heat flow originated in the core, crossed the probe and flew outward into the ambient. Meanwhile, the transverse heat flow also existed. Along the pathway where the heat traveled, the thicker H_{st} became, the more lateral heat loss occurred, leading to an unstable K. Therefore, K could be stabilized by fixing H_{st} and attenuating the transverse heat flow. On the other hand, H_{st} was strongly relevant to the body mass index (BMI) and the probe site. It implied that the placement of the temperature probe should be carefully considered, since H_{st} might vary with different measurement positions and individuals' figures. Thus, the forehead seemed to be a good position since it did not have much adipose tissues and was almost individually uniform. Mendt *et al* (2016) made a large comparison among rectal, skin, and heat flux temperatures

for monitoring circadian rhythms. They also concluded that the sensor site was crucial, with better performance at the forehead compared to the sternum. Furthermore, they demonstrated that the heat flux approach was superior to skin temperature recordings in CBT measurement. Lower T_{air} resulted in a larger temperature difference between the core and the skin (Richmond *et al* 2013). The distribution of subcutaneous fat (Albrecht 2012) also affected skin temperatures, since both the distance from the skin to the core and the thermal conductivity varied with the thickness of skin and fat tissues. Therefore, a mere skin temperature might not be a reliable surrogate for CBT.

The reliability of the CBTMS was highly concerned with the accuracy of the four NTCTs. Huang and Chen (2012) supported the similar suggestion that the estimation of CBT could be improved by increasing the sensor accuracy or deploying more sensors. The four sensors used here had a mean error of 0.009 °C in a wider range of 22–42 °C, compared with that of Huang *et al* (2016) (<0.1 °C in 30–40 °C). Besides, the probe designed by Zhang *et al* (2016) had an average difference of 0.24 °C in a wide range of 22–38 °C with eight sensors adopted, and the error was 1.02 °C with four sensors adopted. Our system was more accurate (average difference 0.08 °C) in 37–41 °C.

The measurement time of the DHF method was usually long due to the lack of active heating process, and isothermal tunnels had to be set up spontaneously. With the help of the proposed reformative material, the initial time was reduced to 23.5 min, which was faster than that of Kitamura *et al* (2010) (30–40 min) and Sim *et al* (2012) (more than 30 min), and was close to that of Huang *et al* (2016) (about 20 min). Here, different materials were attempted. It proved that the heat transfer medium with metal powders (i.e. Ag, Cu) mixed did shorten the thermal equilibrium time, however the temperature gradient between two NTCTs became much smaller as a tradeoff. It was not an optimistic phenomenon when the gradient became too small and (T_{1_meas}, T_{2_meas}), (T_{3_meas}, T_{4_meas}) got too close. T_{core_est} would thereby be more easily miscalculated because of systematic errors. Thus, a sufficiently large temperature difference between two sensors was important to provide adequate measurement accuracy. Calcium carbonate was finally chosen since it offered a quick thermal response as well as enough temperature gradient. Table 1 summarized the comparisons with prior work based on the heat flux methods.

According to the theoretical analysis and the principle of the DHF method, CBT would be properly estimated after thermal equilibrium. The state became unstable when a sporadically strong air flow or sharp temperature fluctuations occurred, meanwhile T_{core_est} could be miscalculated till a new thermal balance. There were common circumstances of sudden temperature changes during daily activities, such as entering/leaving the room, especially in summer/winter with the air conditioner turned on. Thus, the ANC technique utilized here was meaningful for diminishing the artifacts caused by the rapidly changed ambient temperature. Gunga *et al* (2008) employed the temperature obtained at the probe's edge to compensate for ambient temperature changes, and the impact of the forced convection was suppressed significantly according to their calculation.

When the CBTMS applied practically on human subjects, the estimated CBT was comparable with that measured by Nemoto and Togawa (1988) (36.77 ± 0.31 °C versus 36.83 ± 0.13 °C) in similar experimental conditions (room temperature 25 °C, relative humidity 60%, 21 males in rest, measured on the forehead), while the sublingual temperatures were slightly different (36.64 ± 0.12 °C versus 36.84 ± 0.22 °C). Nevertheless, T_{core_est} and T_{sub} were consistent in rest.

The forehead heat flux might be influenced by the superficial blood flow through temporal vessels, especially during acute sports since the blood circulation augmented. The CBTMS was also tested during exercise. Although previous studies were hard to compare due to different experimental protocols, two most comparable were the setups of Teunissen *et al* (2011)

Table 1. Comparisons with prior work.

	Nemoto and Togawa (1988)	Huang *et al* (2016)	Kitamura *et al* (2010)	Sim *et al* (2012)	Zhang *et al* (2016)	This work
Sensor accuracy	/	$<\pm$0.1 °C @ 30–40 °C	/	/	/	0.009 $\pm$ 0.037 °C @ 22–42 °C
Initial response	/	~20 min	30–40 min	>30 min	/	~23.5min
Probe test on hot plate / water bath	$<\pm$0.1 °C @ 37 °C	/	<0.1 °C @37 °C	Carried out in water bath, accuracy not mentioned	0.24 °C @ 22–38 °C, 8 sensors; 0.35 °C @ 22–38 °C, 6 sensors; 1.02 °C @ 22–38 °C, 4 sensors	0.08 $\pm$ 0.20 °C @ 37–41 °C

(10 min rest, 30 min cycling and 10 min recovery) and Huang *et al* (2016) (30 min rest, 15 min exercise and 10 min recovery). The temperature pattern of the estimated CBT in this approach was similar to the studies mentioned above.

However, most previous work (Teunissen *et al* 2011, Brandes *et al* 2015, Huang *et al* 2016) was carried out indoors under the climate controlled environment such as a thermostatic and windless chamber, since winds would bring the interference for those heat flux based CBT measurements. In contrast, subjects here could jog outdoors freely and the change of CBT could be reflected under windy conditions by the proposed wireless system and ANC technique.

The application of T_{sub} was advised against during exercise above 35% VO_{2max} (Blatteis 1998) due to saliva and ventilation interference, which meant T_{sub} was not a reliable reference during jogging. Thus, the comparative results of T_{core_est} and T_{sub} were not shown in this paper. Here, only a pilot study was demonstrated to observe the performance of the CBTMS, and oesophageal/rectal temperatures will be used as references to validate its accuracy under field conditions.

During the trials, participants claimed no discomfort after the probe attached to the forehead over hours. Thanks to the properties of viscoelasticity, biocompatibility and high hydrophobicity of PDMS, the probe used here was suitable for long-term monitoring without arousing skin allergies. The wearable CBTMS had the potential for continuous CBT monitoring.

5. Conclusion

A miniaturized CBTMS based on the DHF and ANC methods was designed and implemented. Besides, a reformative heat transfer medium was applied to accelerate the thermal response, while a LMS adaptive filter was adopted to prevent the CBTMS from being influenced by ambient temperature fluctuations.

The results suggested that the CBTMS could measure CBT noninvasively and transmit data wirelessly. The miniaturization made it convenient to be worn as a hairlace without hindering

normal activities. The equilibrium time was shorter than some previous studies based on the DHF method, and the impact of air temperature fluctuations was mitigated by the proposed ANC technique. Despite these improvements, the equilibrium and recovery time was still probably long for some applications. Thus, embedded algorithms to predict CBT could be studied, which would benefit faster measurements. The CBTMS was preliminarily tested on humans as a pilot in this work, and experiments using oesophageal/rectal temperatures as references will be conducted to validate the performance of our system in the future.

Acknowledgment

This work was supported by National Science and Technology Major Project of the Ministry of Science and Technology of China (No.2013ZX03005008).

Appendix

The principle of LMS adaptive filter

Figure A1 showed the diagram of LMS adaptive filter algorithm. $x(n)$ was the input signal which worked as reference. $d(n)$ was the corrupted signal. $y(n)$ regarded as the estimated artifacts, was the output signal which could be calculated by equation (A.1).

$$y(n) = \sum_{i=1}^{M} w(i)x(n-i+1) \tag{A.1}$$

Where $w(n)$ was the adjustable weight coefficient of the filter, and should be updated every loop by equation (A.2).

$$w(n+1) = w(n) - 2\mu e(n)x(n) \tag{A.2}$$

Where μ was the step size, $e(n)$ was derived from $e(n) = d(n) - y(n)$. The adaptive filter was optimized when the minimized $e(n)$ was obtained under certain criterion. In this study, $x(n)$ was known as the fluctuated ambient temperature and $d(n)$ was regarded as one of the temperatures T_1–T_4 measured by thermometers.

The principle of CBT measurement

According to the Fourier's law of heat conduction shown as equation (A.3), the time rate of heat transfer through a material was proportional to the negative gradient in the temperature and to the area (Lienhard and Lienhard 2006).

$$q = -\lambda \frac{\partial T}{\partial x} \tag{A.3}$$

Where q, λ were the heat flux (W m^{-2}) and the thermal conductivity (W $m^{-1} \cdot K$), respectively. For a three-dimension general heat conduction, the change rate of energy content of the element included three parts: (1) the rate of heat conduction at x, y, and z; (2) the rate of heat conduction at $x + \Delta x$, $y + \Delta y$, and $z + \Delta z$; (3) the rate of heat generation inside the element. It could be described as equation (A.4) (Lienhard and Lienhard 2006).

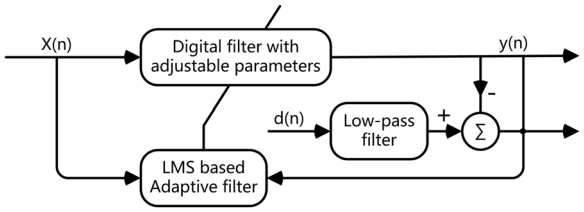

Figure A1. The diagram of LMS adaptive filter.

$$\rho c\frac{\partial T}{\partial \tau}=\frac{\partial}{\partial x}\left(\lambda\frac{\partial T}{\partial x}\right)+\frac{\partial}{\partial y}\left(\lambda\frac{\partial T}{\partial y}\right)+\frac{\partial}{\partial z}\left(\lambda\frac{\partial T}{\partial z}\right)+\overline{\Phi} \tag{A.4}$$

Where ρ, c, τ, and $\overline{\Phi}$ were the density of element (kg m^{-3}), the specific heat capacity (J $kg^{-1}\cdot$ K), time and the rate of heat generation inside the element, respectively.

For the model (figure 3) with no internal heat generation from the probe in a steady-state, equation (A.4) could be simplified and solved with related initial and boundary conditions when taking the vertical heat flow I_1 into account.

$$\begin{cases}\dfrac{\partial^2 T}{\partial z^2}=0\\ T\Big|_{z=0}=T_{\text{core}}\Rightarrow T=T_{\text{core}}+\dfrac{T_1-T_{\text{core}}}{l_1}z, z\in[0,l_1]\\ T\Big|_{z=l_1}=T_1\end{cases} \tag{A.5}$$

Where T_{core} was the CBT, T was the temperature distribution along l_1 (vertical direction). Combining equation (A.3) with equation (A.5), the heat transfer rate Φ (Lienhard and Lienhard 2006) could be derived as equation (A.6).

$$\Phi=qA=-\lambda\frac{T_1-T_{\text{core}}}{l_1}A=\frac{\Delta T}{R}, R=\frac{1}{\lambda A} \tag{A.6}$$

Where R was defined as the thermal resistance. ΔT was the temperature difference along z axis. Heat flux 1 from the deep tissue to the surface of the skin and subcutaneous tissue layer, and Heat flux 2 from the skin and subcutaneous tissue layer to the surface of the probe should be same after thermal equilibrium. Thus from equation (A.6), we could draw the conclusion as follows.

$$\frac{T_{\text{core}}-T_1}{R_s}=\frac{T_1-T_2}{R_1}\Rightarrow T_{\text{core}}=T_1+\frac{R_s}{R_1}(T_1-T_2) \tag{A.7}$$

Similarly to Channel 1, CBT could also be estimated by using the heat flux in Channel 2.

$$T_{\text{core}}=T_3+\frac{R_s}{R_2}(T_3-T_4) \tag{A.8}$$

When combining equations (A.7) and (A.8), R_s, which was individual-dependent, was eliminated. Noting that R_s in both Channel 1 and 2 were assumed to be approximately equal, since two measured channels were usually close or symmetrical to each other in application. Hence equation (1) was derived.

References

Albrecht U 2012 Timing to perfection: the biology of central and peripheral circadian clocks *Neuron* **74** 246–60

Bland J M and Altman D G 1995 Comparing methods of measurement: why plotting difference against standard method is misleading *Lancet* **346** 1085–7

Blatteis C 1998 Methods of body temperature measurement *Physiology and Pathophysiology of Temperature Regulation* (River Edge, NJ: World Scientific) pp 273–9

Brandes I F, Perl T, Bauer M and Bräuer A 2015 Evaluation of a novel noninvasive continuous core temperature measurement system with a zero heat flux sensor using a manikin of the human body *Biomed. Eng.* **60** 1–9

Byrne C and Lim C L 2007 The ingestible telemetric body core temperature sensor: a review of validity and exercise applications *Br. J. Sports Med.* **41** 126–33

Conti B, Tabarean I, Andrei C and Bartfai T 2004 Cytokines and fever *Front. Biosci.* **9** 1433–49

Epstein Y and Roberts W 2011 The pathopysiology of heat stroke: an integrative view of the final common pathway *Scand. J. Med. Sci. Sports* **21** 742–8

Eshraghi Y, Nasr V, Parra-Sanchez I, Van Duren A, Botham M, Santoscoy T and Sessler D I 2014 An evaluation of a zero-heat-flux cutaneous thermometer in cardiac surgical patients *Anesth. Analg.* **119** 543–9

Fox R, Solman A, Isaacs R, Fry A and MacDonald I 1973 A new method for monitoring deep body temperature from the skin surface *Clin. Sci.* **44** 81–6

Freedman R R 2014 Menopausal hot flashes: mechanisms, endocrinology, treatment *J. Steroid Biochem. Mol. Biol.* **142** 115–20

Gunga H-C, Sandsund M, Reinertsen R E, Sattler F and Koch J 2008 A non-invasive device to continuously determine heat strain in humans *J. Therm. Biol.* **33** 297–307

Gunga H C, Werner A, Stahn A, Steinach M, Schlabs T, Koralewski E, Kunz D, Belavy D L, Felsenberg D, Sattler F and Koch J 2009 The double sensor-A non-invasive device to continuously monitor core temperature in humans on earth and in space *Respir. Physiol. Neurobiol.* **169** S63–8

Höcker J, Bein B, Böhm R, Steinfath M, Scholz J and Horn E-P 2012 Correlation, accuracy, precision and practicability of perioperative measurement of sublingual temperature in comparison with tympanic membrane temperature in awake and anaesthetised patients *Eur. J. Anaesthesiol.* **29** 70–4

Han H and Kim J 2012 Artifacts in wearable photoplethysmographs during daily life motions and their reduction with least mean square based active noise cancellation method *Comput. Biol. Med.* **42** 387–93

Hansen C N 2002 *Understanding Active Noise Cancellation* (Boca Raton, FL: CRC Press)

Haykin S and Widrow B 2003 *Least-Mean-Square Adaptive Filters* vol 31 (New York: Wiley)

Hooper V D and Andrews J O 2006 Accuracy of noninvasive core temperature measurement in acutely ill adults: the state of the science *Biol. Res. Nursing* **8** 24–34

Huang M and Chen W 2010 Theoretical simulation of the dual-heat-flux method in deep body temperature measurements *2010 Annual Int. Conf. of the IEEE Engineering in Medicine and Biology Society (EMBC)* (IEEE) pp 561–4

Huang M and Chen W 2012 Theoretical study on the inverse modeling of deep body temperature measurement *Physiol. Meas.* **33** 429

Huang M, Tamura T, Tang Z, Chen W and Kanaya S 2016 A wearable thermometry for core body temperature measurement and its experimental verification *IEEE J. Biomed. Health Inform.* https://doi.org/10.1109/JBHI.2016.2532933

Kitamura K-I, Zhu X, Chen W and Nemoto T 2010 Development of a new method for the noninvasive measurement of deep body temperature without a heater *Med. Eng. Phys.* **32** 1–6

Kolka M A, Quigley M D, Blanchard L A, Toyota D A and Stephenson L A 1993 Validation of a temperature telemetry system during moderate and strenuous exercise *J. Therm. Biol.* **18** 203–10

Lienhard IV J H and Lienhard V J H 2006 *A heat transfer textbook* (Cambridge, Massachusetts: Phlogiston Press)

Mendt S, Maggioni M A, Nordine M, Steinach M, Opatz O, Belavý D, Felsenberg D, Koch J, Shang P and Gunga H-C 2016 Circadian rhythms in bed rest: monitoring core body temperature via heat-flux approach is superior to skin surface temperature *Chronobiol. Int.* 1–11

Nemoto T and Togawa T 1988 Improved probe for a deep body thermometer *Med. Biol. Eng. Comput.* **26** 456–9

Nybo L, Rasmussen P and Sawka M N 2014 Performance in the heat—physiological factors of importance for hyperthermia-induced fatigue *Compr. Physiol.* **4** 657–89

Richmond V, Wilkinson D, Blacker S, Horner F, Carter J, Havenith G and Rayson M 2013 Insulated skin temperature as a measure of core body temperature for individuals wearing CBRN protective clothing *Physiol. Meas.* **34** 1531

Satlin A, Volicer L, Stopa E G and Harper D 1995 Circadian locomotor activity and core-body temperature rhythms in Alzheimer's disease *Neurobiol. Aging* **16** 765–71

Saurabh K, Rao H, Amrutur B and Sundarrajan A 2014 Continuous core body temperature estimation via surface temperature measurements using wearable sensors is it feasible? *Conf.: BIODEVICES 2014, 7th Int. Conf. on Biomedical Electronics and Systems (At Esio, Angers, Loire Valley, France)*

Sim S Y, Lee W K, Baek H J and Park K S 2012 A nonintrusive temperature measuring system for estimating deep body temperature in bed *2012 Annual Int. Conf. of the IEEE Engineering in Medicine and Biology Society (EMBC)* pp 3460–3

Steck L N, Sparrow E M and Abraham J P 2011 Non-invasive measurement of the human core temperature *Int. J. Heat Mass Transfer* **54** 975–82

Teunissen L, de Haan A, de Koning J and Daanen H 2012 Telemetry pill versus rectal and esophageal temperature during extreme rates of exercise-induced core temperature change *Physiol. Meas.* **33** 915

Teunissen L, Klewer J, De Haan A, De Koning J and Daanen H 2011 Non-invasive continuous core temperature measurement by zero heat flux *Physiol. Meas.* **32** 559

Yamakage M and Namiki A 2003 Deep temperature monitoring using a zero-heat-flow method *J. Anesth.* **17** 108–15

Yuan P 2009 Numerical analysis of an equivalent heat transfer coefficient in a porous model for simulating a biological tissue in a hyperthermia therapy *Int. J. Heat Mass Transfer* **52** 1734–40

Zhang Y, Chad Webb R, Luo H, Xue Y, Kurniawan J, Cho N H, Krishnan S, Li Y, Huang Y and Rogers J A 2016 Theoretical and experimental studies of epidermal heat flux sensors for measurements of core body temperature *Adv. Healthc. Mater.* **5** 119–27